Article

Methanol Oxidation Using Ternary Ordered Intermetallic Electrocatalysts: A DEMS Study

Rui Zeng, Yao Yang, Tao Shen, Hongsen Wang, Yin Xiong, Jing Zhu, Deli Wang, and Héctor D. Abruña

ACS Catal., **Just Accepted Manuscript** • DOI: 10.1021/acscatal.9b04344 • Publication Date (Web): 05 Dec 2019

Methanol Oxidation Using Ternary Ordered Intermetallic Electrocatalysts: A DEMS Study

Rui Zeng,[†] Yao Yang,[†] Tao Shen,[‡] Hongsen Wang,[†] Yin Xiong,[†] Jing Zhu,[‡]

Deli Wang,*[,‡] Héctor D. Abruña*[,†]

[†]Department of Chemistry and Chemical Biology, Baker Laboratory, Cornell University, Ithaca, New York 14853, United States

[‡]Key laboratory of Material Chemistry for Energy Conversion and Storage, Ministry of Education, Hubei Key Laboratory of Material Chemistry and Service Failure, School of Chemistry and Chemical Engineering, Huazhong University of Science and Technology, Wuhan 430074, P. R. China

ABSTRACT

The sluggish methanol oxidation reaction (MOR) remains the biggest challenge for direct methanol fuel cells. To advance our understanding of the MOR mechanism, we have employed dual thin-layer differential electrochemical mass spectrometry (DEMS) to study reaction intermediates on a family of Pt-Fe-Cu ternary ordered intermetallics. We found that $PtFe_{0.7}Cu_{0.3}/C$ exhibited the highest CO_2 production efficiency, while $PtFe_{0.5}Cu_{0.5}/C$ generated the largest proportion of methyl formate or formic acid. The different selectivity is partially ascribed to the difference in lattice compressive strain due to the incorporation of Fe and Cu atoms. We propose a dual-pathway mechanism in which the increase in lattice contraction can stabilize the intermediates forming methyl formate or formic acid, while a moderate lattice strain leads to the highest CO_2 generation via CO_{ad} intermediates. Our work on ternary catalysts may provide valuable insights for designing electrocatalysts for the MOR.

KEYWORDS

direct methanol fuel cells, methanol oxidation, methyl formate, formic acid, DEMS, ordered intermetallics

Introduction:

Direct Methanol Fuel Cells (DMFCs) have received a great deal of attention due to their high energy conversion efficiency and portability.[1-2] However, the methanol oxidation reaction (MOR) in DMFCs is challenging since intermediate species such as CO_{ad} can poison the reaction active sites, hindering further conversion to CO_2.[2] Platinum has been shown to be the most active monometallic catalyst for the MOR, but a high Pt loading is still required at high overpotentials to oxidatively remove CO_{ad} species. By alloying Pt with other non-precious metals, it is possible to lower the loading of Pt and mitigate the overpotential by introducing a bifunctional mechanism,[3] electronic effects,[4] or third-body effects.[5,6] Pt-Ru alloys[7] are regarded as model catalysts for the MOR since the onset potential can be 200-300 mV lower than Pt.[8] However, the Pt-Ru alloys still suffer from significant overpotentials and poor durability.[6,9] Ordered intermetallic catalysts have higher leaching resistance in acidic conditions due to their higher formation energy relative to the disordered counterparts.[10] As a result, Pt-based ordered intermetallics have been intensively investigated as promising catalysts in electrocatalysis.[11] Previously, Pt-Pb,[12] Pt-Zn,[10,13] Pt-Ti and Pt-V[14] intermetallic nanocatalysts have been reported to exhibit superior MOR performance relative to Pt. Recently, we have reported a systematic study on a family of Pt-Fe-Cu electrocatalysts, with ordered intermetallic structures and a 2-3 atomic layer Pt-skin. They showed significantly enhanced activity and durability for the MOR, when compared to the disordered counterparts and Pt/C.[15]

Differential electrochemical mass spectrometry (DEMS) is a powerful tool for detecting gaseous or volatile species. Depending on the type of the electrochemical cell, DEMS has several basic designs: conventional cell, thin-layer cell, dual thin-layer flow cell and capillary inlet.[16,17] Among them, the dual thin-layer flow cell has received extensive attention for its capability of being coupled to other analytical tools, such as attenuated total reflection-infrared spectroscopy (ATR-FTIRS)[18,19] and electrochemical quartz crystal microbalance (EQCM).[20] Compared to conventional electrochemical methodologies, which use only overall current density as a metric to evaluate the MOR performance, DEMS offers not only detection of specific species, but also quantitative descriptors for evaluating catalyst activity and especially selectivity. Herein, we report on an in-depth DEMS-study of the MOR mechanism on Pt-Fe-Cu ternary catalysts.

RESULTS AND DISCUSSION

Pt-Fe-Cu ternary ordered intermetallics were prepared by an impregnation method under a flowing H_2 gas atmosphere. X-ray diffraction (XRD) (Figure 1A) and high-angle annular dark-field scanning transmission electron microscopy (HAADF-STEM) (Figures 1B-C) were employed to characterize the structure and morphology of the Pt-Fe-Cu electrocatalysts. Compared to Pt/C (Figure S1), the XRD patterns of Pt-Fe-Cu catalysts exhibited the features of a tetragonal PtFe ordered intermetallic, similar to the standard XRD pattern of PtFe (PDF #01-089-2051). $PtFe_{0.5}Cu_{0.5}$/C showed a positive shift in the (001) planes when compared to PtFe/C (Figure 1A), indicating that the partial replacement of Fe by Cu causes a lattice contraction in ***c*** due to the smaller size of Cu relative to Fe. An expansion in the ***a*** direction, as observed from the (100) plane (Table S1) is likely an adjustment to the change of the unit cell in the ***c*** direction.[15] Atomic-scale STEM images of $PtFe_{0.5}Cu_{0.5}$ exhibited a 3.7 Å lattice d-spacing, which was assigned to the (001) facet, based on PDF #01-089-2051 (Figures 1B-C). The brighter atom columns are Pt atoms while the dimmer atoms are M (Fe or Cu) since the HAADF-STEM image intensity is proportional to atomic number ($I \propto Z^{1.7}$). Atomic-scale STEM images of $PtFe_{0.5}Cu_{0.5}$ along the [010] zone axis exhibited a 2-3 atomic-layer of pure Pt shell on the surface (Figure S2). The above image analysis convincingly suggests that the as-prepared catalysts are an ordered intermetallic phase, consistent with the XRD results.

As shown in Figure 2A, the DEMS setup is composed of three components: electrochemical cell, porous Teflon membrane and vacuum chamber, which is connected to the mass spectrometer. Generally, under an applied potential, gaseous or volatile species, generated at the surface of the working electrode, are carried away by the incoming electrolyte flux from the inlet and diffuse through the gas-permeable porous membrane. The rest of the solution is pumped out to the outlet using a syringe pump.

The top panel in Figure 2B presents the cyclic voltammetric (CV) profile at 10 mV/s of Pt/C in a 0.2M methanol solution in Ar saturated 0.2M $HClO_4$ while the middle and bottom panels present the mass spectrometric (MS) signals of CO_2 (m/z=44) and methyl formate (m/z=60), respectively, as a function of applied potential. Although they can be main byproducts, the MS signals for formic acid (m/z=46) and formaldehyde (m/z=30) are not presented since they overlap with the MS signals from CO_2 and methanol, respectively [21,22]. Therefore, we use the m/z=60 signal (methyl formate) as proxy for the generation of formic acid[23,22]. The m/z=44 ion current closely follows the faradaic current profile while the m/z=60 ion current has a clear delay in the reverse scan (bottom panel in Figure 2B), which is likely due to the slow kinetics of methyl formate formation.[22,24] (Time delays (2~3 s at a flow rate of 10 μL/s) between the generation and detection of specific species can be seen in Figure S3.) The m/z=44 ion current was calibrated via formic acid oxidation at 0.70 V vs. RHE (Figure 2C) while the calibration of m/z=60 was performed based on m/z=44 and m/z=60 (see DEMS calibration section in Supporting Information for details). It is interesting to note that the signal delay between m/z=60 and m/z=44 was about 0.5 s (Figure 2D), possibly due to the difference in partition coefficients between methyl formate and CO_2 in the Teflon membrane.

After calibration of the DEMS setup, CO stripping cyclic voltammograms were performed to characterize the CO tolerance of the catalysts (Figures 3A-B). In the first half cycle, the hydrogen desorption region is significantly suppressed due to the saturation coverage of CO on the catalyst surface. The broad current peaks, corresponding to CO oxidation, are generally found between 0.7 and 0.9 V. PtFe/C, $PtFe_{0.5}Cu_{0.5}$/C and $PtFe_{0.7}Cu_{0.3}$/C all have negatively shifted peak positions, relative to Pt/C, indicating a higher tolerance against CO-poisoning (weaker CO binding), which is consistent with our previous work.[15] Based on the CO_2 partial current density (derived from the MS signal at m/z=44) in Figure 3B, PtFe and Pt-Fe-Cu catalysts have significantly lower onset potentials, relative to Pt/C, likely due to a weaker CO adsorption, again, consistent with the above.[25] Interestingly, the overall current density in Figure 3A is larger than the CO_2 partial current density. Charge integration of the peak current density reveals that the CO_2 current density represents about 75% of the total current density, indicating a 25% contribution from non-faradaic processes, most likely due to anion re-adsorption during CO stripping.[19] These results highlight the unique capabilities of DEMS in establishing the faradaic processes, when compared to the limited information derived from the overall current in CV profiles.

The MOR was further studied under potentiodynamic cyclic voltammetry. The CO_2 current densities presented in Figure 4A, follow the same trend as the total current density in Figure S4. In the CV profile, the first peak, corresponding to the anodic oxidation of methanol, appears at around 0.9 V in the positive scan while in the reverse (cathodic) scan a peak can be found at around 0.7 V. Interestingly, all of the catalysts, except Pt/C, exhibited a decreased peak intensity in the negative scan direction, when compared to the positive scan direction. This discrepancy is likely due to different reactivation efficiencies of the catalysts.[26] When comparing CO_2 conversion efficiencies, all the catalysts exhibited an overall value of around 70% (Figure 4B). Among the catalysts, even though PtFe/C presented the highest overall current density for MOR, $PtFe_{0.7}Cu_{0.3}/C$ exhibited a slightly higher overall yield for CO_2 (71.4 ± 4.2%), relative to other compositions. Notably, regardless of the compositions of the catalysts, the conversion efficiency of CO_2 in the negative scan was consistently larger than that in the positive scan (Figure 4B). This behavior can be explained by the chemical reaction between Pt-oxide species and methanol in the negative scan, which generates CO_2 without producing a faradaic current response.[22] Again, this illustrates the value of DEMS in such mechanistic studies. The methyl formate ion current (Figure 4C) is about two orders of magnitude lower than CO_2, mainly due to its slow reaction rate.[23] Similar to the behavior of CO_2, methyl formate presents peaks at around 0.9 V and 0.7 V in the positive and negative scans, respectively, with the first peak being significantly larger than the second, except for Pt/C. As shown in Figure 4D, $PtFe_{0.5}Cu_{0.5}/C$ has the highest methyl formate conversion efficiency (2.1 ± 0.1%), relative to other compositions. It is possible to calculate the generation rate of formic acid from methyl formate assuming that an equilibrium exists between methyl formate and formic acid.[23,27] However, a quantitative measurement of formic acid formation rate is challenging with DEMS.[28] Nevertheless, a qualitative assessment is still valuable as a higher yield of methyl formate indicates a larger amount of formic acid formed.

To further investigate the reaction mechanism, chronoamperometric (CA) curves were performed to evaluate the catalyst's CO tolerance and stability. The generation of CO_2 and methyl formate at 0.80 V exhibited a noticeable decay (Figures 5A-B), which is unlikely due to CO-poisoning effects since CO_{ad} is believed to be completely oxidized at such high overpotentials (Figure 3). A similar behavior has been reported for single-crystalline[29] and polycrystalline Pt electrodes.[30] The decrease was attributed to the gradual deactivation of the platinum surface by water and/or anion adsorption.[29] The periodic fluctuations present in the profiles are mainly due to the use of peristaltic syringe pump, which causes a discontinuous motion of the solution. Subtracting the contribution of the CO_2 current from the total current density yields a combination of formic acid and formaldehyde (Figure 5C), since CO_2, formic acid and formaldehyde are the main products. The rapid initial decay of the current is likely due to the pseudocapacitive double layer discharging and smearing effect from the electrolyte's mass transport.[22] In contrast to the gradual decay in CO_2 or methyl formate (Figures 5A-B), the combined current of formic acid and formaldehyde remains virtually constant over the entire time period, indicating that CO_2 generation dominates the current decay in the chronoamperometric profiles. The current efficiencies of CO_2 and methyl formate were calculated by choosing signals at 120 s, as shown in Figure 5D. Consistent with the results of the potentiodynamic study, $PtFe_{0.7}Cu_{0.3}/C$ exhibited a slightly higher conversion efficiency for CO_2 production ($74.2 \pm 3.2\%$) while $PtFe_{0.5}Cu_{0.5}/C$ exhibited the highest yield for methyl formate ($2.4 \pm 0.1\%$) or formic acid. Overall, the potentiodynamic and potentiostatic studies were well consistent with each other.

Based on previous work[31,32,28,33] and as well as on our experiment results, we propose a possible reaction mechanism as shown in Scheme 1. The first step involves breaking of a C-H bond, producing H_2COH_{ad}, some of which can be converted to formaldehyde. The adsorbed H_2COH can be further dehydrogenated to $HC{=}O_{ad}$, which plays an important role in determining whether the reaction goes through the indirect or direct pathway. At low potentials (< 0.7 V), when adsorbed CO species are very stable, the reaction is dominated by the direct pathway[33] producing HCOOH or $HCOOCH_3$ at the surface of the electrode.

The generation of $HCOOCH_3$ may be induced by an esterification reaction with CH_3OH catalyzed by Pt on the surface of the electrode.[30] However, based on the rather long time constant (1×10^5 s) of esterification between HCOOH and CH_3OH on polycrystalline Pt electrode, Baltruschat et al. proposed that methyl formate should be formed at the electrode/electrolyte interface by nucleophilic attack of CH_3O^- species on $HC{=}O_{ad}$.[28] However, it remains challenging to translate such a finding, on a smooth polycrystalline electrode, into nano-sized catalysts, since the electric field, local pH, methanol concentration and mass transport conditions on different nanocatalyst facets can be (and likely are) significantly different. Therefore, it is possible that esterification still has some contribution to the formation of methyl formate on nano-sized catalysts. Therefore, we have included both mechanisms in our Scheme 1. The coexistence of two methyl formate formation mechanisms does not compromise our analysis on formic acid, since in the nucleophilic attack case, the ratio of formic acid to methyl formate should be determined by their ratio of nucleophilic power, which should be a constant independent of potential.[28] The generated species on the surface of the electrode, H_2CO_{surf}, $HCOOH_{surf}$ and $HCOOCH_{3surf}$, can diffuse away from the electrode.

When the applied potential is high enough to oxidatively remove adsorbed CO, the reaction occurs through both direct and indirect pathways. The $HCOOH_{surf}$ can be converted to CO_2 via CO_{ad} or directly, as indicated by previous work.[6,33] However, whether the reaction goes through the direct or indirect pathway depends on the nature of the electrode surface. If the surface of the electrode can stabilize the transition states during the conversion from $HC{=}O_{ad}$ to $HCOOH_{surf}$ or $HCOOCH_{3surf}$, then the direct pathway will be favored. In Figure 5D, it is interesting to note that the conversion efficiency of methyl formate increases monotonically with an increase in the lattice contraction. This is probably due to the strained Pt lattice which serves as a stabilizer toward the transition-state intermediates ($HC(OH)_{2ad}$ or $HCOHOCH_{3ad}$), explaining why $PtFe_{0.5}Cu_{0.5}/C$ exhibits the highest activity to produce formic acid or methyl formate. The change in the efficiency of CO_2 production appears to be nonmonotonic. A moderate increase in the lattice contraction is believed to weaken the CO binding energy, which can facilitate CO oxidation to CO_2.[34] However, if the lattice contraction is too strong, to such an extent that CO cannot easily adsorb to the surface, the generation of CO_2 via CO therefore will be hindered, yielding a lower efficiency. This explanation reveals why a further lattice contraction from $PtFe_{0.7}Cu_{0.3}/C$ to $PtFe_{0.5}Cu_{0.5}/C$ leads to a slight decrease in the CO_2 production efficiency. These observations and interpretations offer a reasonable answer to the behaviors of those catalysts although they still need to be corroborated by theoretical calculations which is part of our future work.

CONCLUSIONS

In conclusion, we have studied the MOR on Pt-Fe-Cu ternary alloy catalysts using DEMS. Our results indicate that $PtFe_{0.7}Cu_{0.3}/C$ possesses the highest conversion efficiency of CO_2 while $PtFe_{0.5}Cu_{0.5}/C$ exhibits the maximum yield of methyl formate or formic acid. Based on our proposed mechanism, the increased production of methyl formate or formic acid is due to the stabilizing effect of the lattice strain on transition-state intermediates, while the nonmonotonic dependence of CO_2 efficiency on lattice strain indicates that the CO binding energy should be at a moderate level. This work provides possible structure-activity correlations for the MOR electrocatalysts and may help understand and unravel the complex MOR reaction mechanism.

ASSOCIATED CONTENT

Supporting Information

The Supporting Information is available free of charge on the ACS Publications website at DOI: xx. Synthesis, structural characterizations of XRD, STEM, and electrochemical characterizations, including Table S1 and Figures S1-S5 (PDF).

AUTHOR INFORMATION

Corresponding Authors

*E-mail: hda1@cornell.edu

*E-mail: wangdl81125@hust.edu.cn

ORCID

Rui Zeng: 0000-0002-7577-767X

Yao Yang: 0000-0003-0321-3792

Hongsen Wang: 0000-0001-7926-2895

Deli Wang: 0000-0003-2023-6478

Héctor D. Abruña: 0000-0002-3948-356X

Notes

The authors declare no competing financial interests.

ACKNOWLEDGEMENT

This work was supported by the Air Force Office of Scientific Research under award number FA9550-18-1-0420. Atomic-scale STEM images were acquired using of TEM facilities of the Cornell Center for Materials Research (CCMR) which are supported through the National Science Foundation Materials Research Science and Engineering Center (NSF MRSEC) program (DMR-1719875). In addition, the synthesis part of this work was supported by the National Natural Science Foundation of China (21573083).

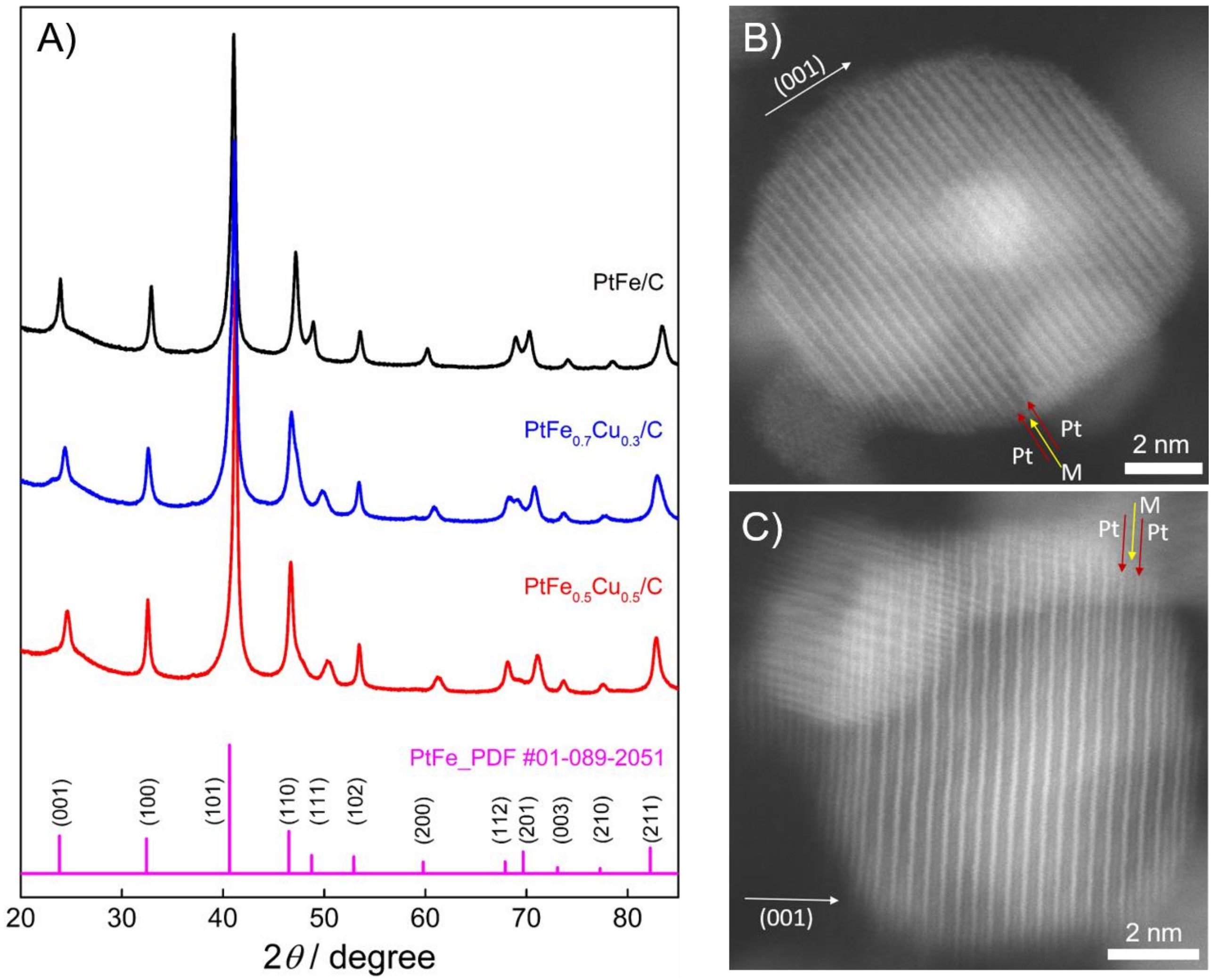

Figure 1. (A) XRD patterns for PtFe/C, $PtFe_{0.7}Cu_{0.3}/C$ and $PtFe_{0.5}Cu_{0.5}/C$. The magenta vertical lines indicate the peak positions of standard XRD patterns of ordered PtFe. (B-C) Atomic-scale STEM images of $PtFe_{0.5}Cu_{0.5}/C$. Red and yellow arrows indicate the direction of Pt and M (Fe, Cu) atoms, respectively.

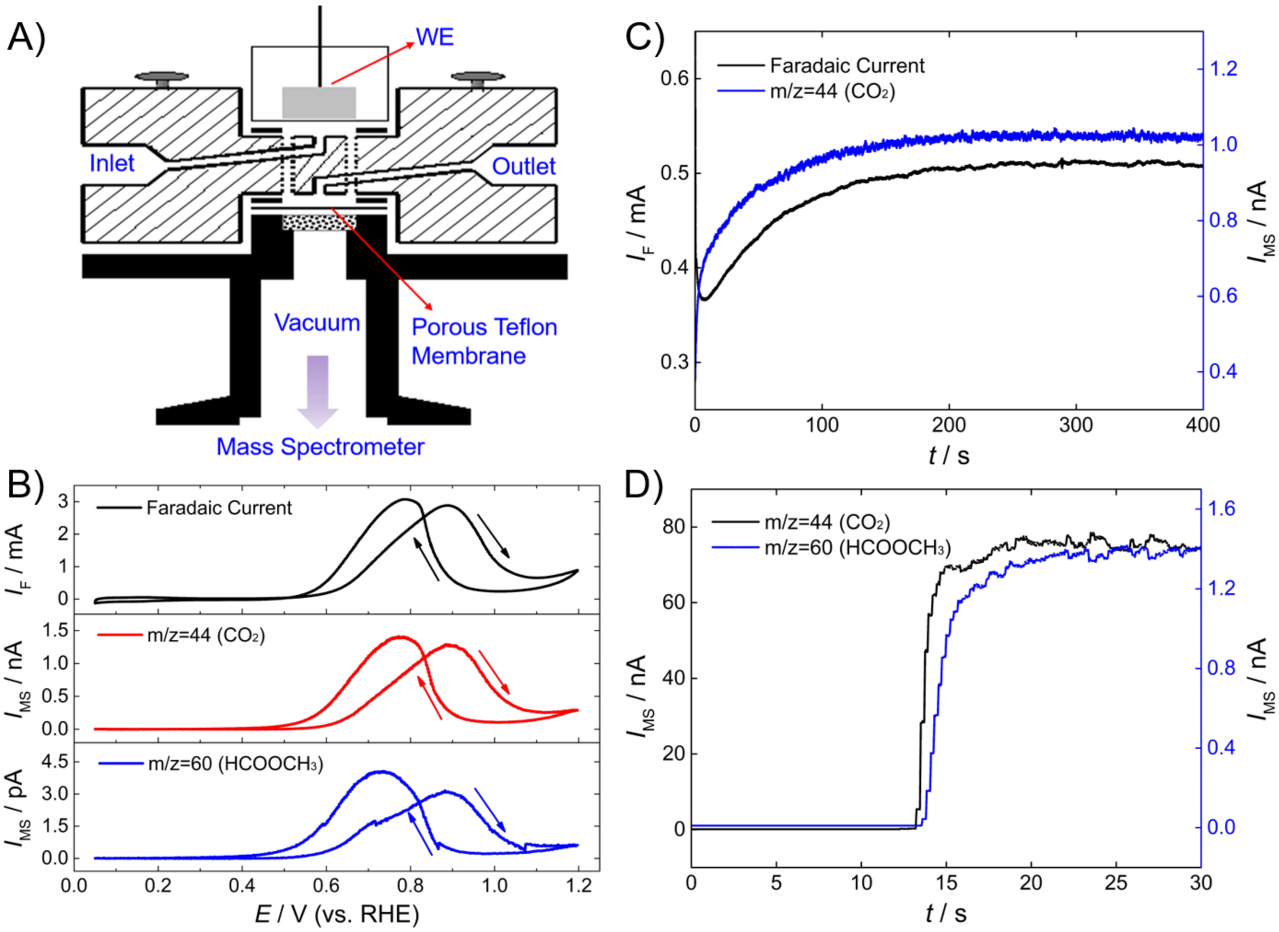

Figure 2. (A) A schematic of the dual thin-layer DEMS setup. (B) CV profiles and MSCV profiles for methanol oxidation at m/z=44 and m/z=60, recorded on Pt/C in Ar-saturated 0.2 M $HClO_4$ and 0.2 M CH_3OH, scan rate: 10 mV/s. Arrows indicate the direction of the profiles. (C) Chronoamperometry for formic acid oxidation on Pt/C, in Ar-saturated 0.2 M $HClO_4$ and 10 mM HCOOH at 0.70 V vs. RHE. (D) Mass spectrometric signals collected from saturated CO_2 and 10 mM methyl formate in aqueous solution. Flow rate:10 μL/s.

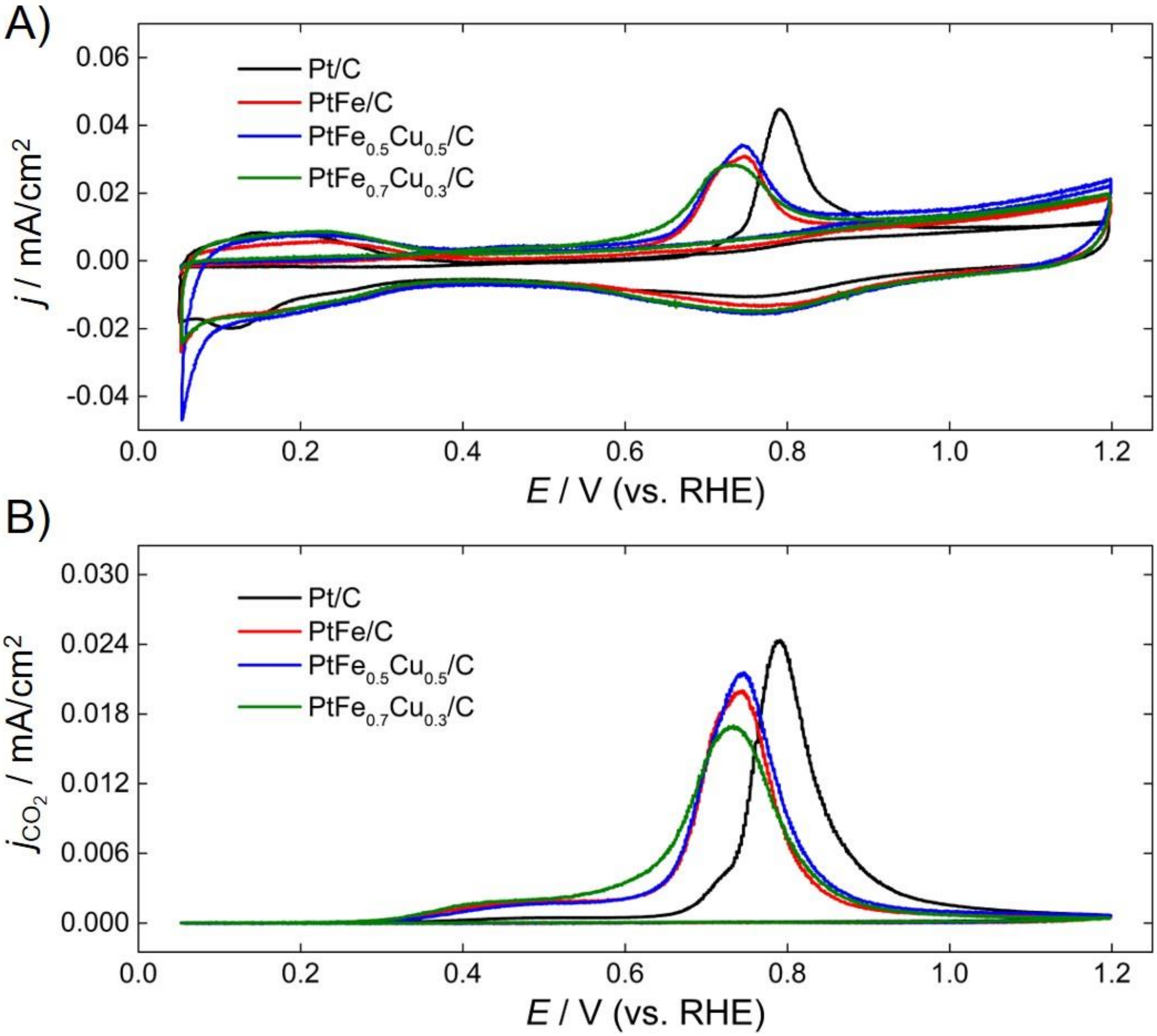

Figure 3. CO stripping voltammograms: (A) Overall electrochemical current density. (B) CO_2 partial current density, derived from MS signal at m/z=44. Scan rate: 10 mV/s, Flow rate: 10 μL/s. All the currents were normalized to the electrochemical surface area (ECSA). Negative shifts of onset and peak potentials indicate higher CO-tolerance.

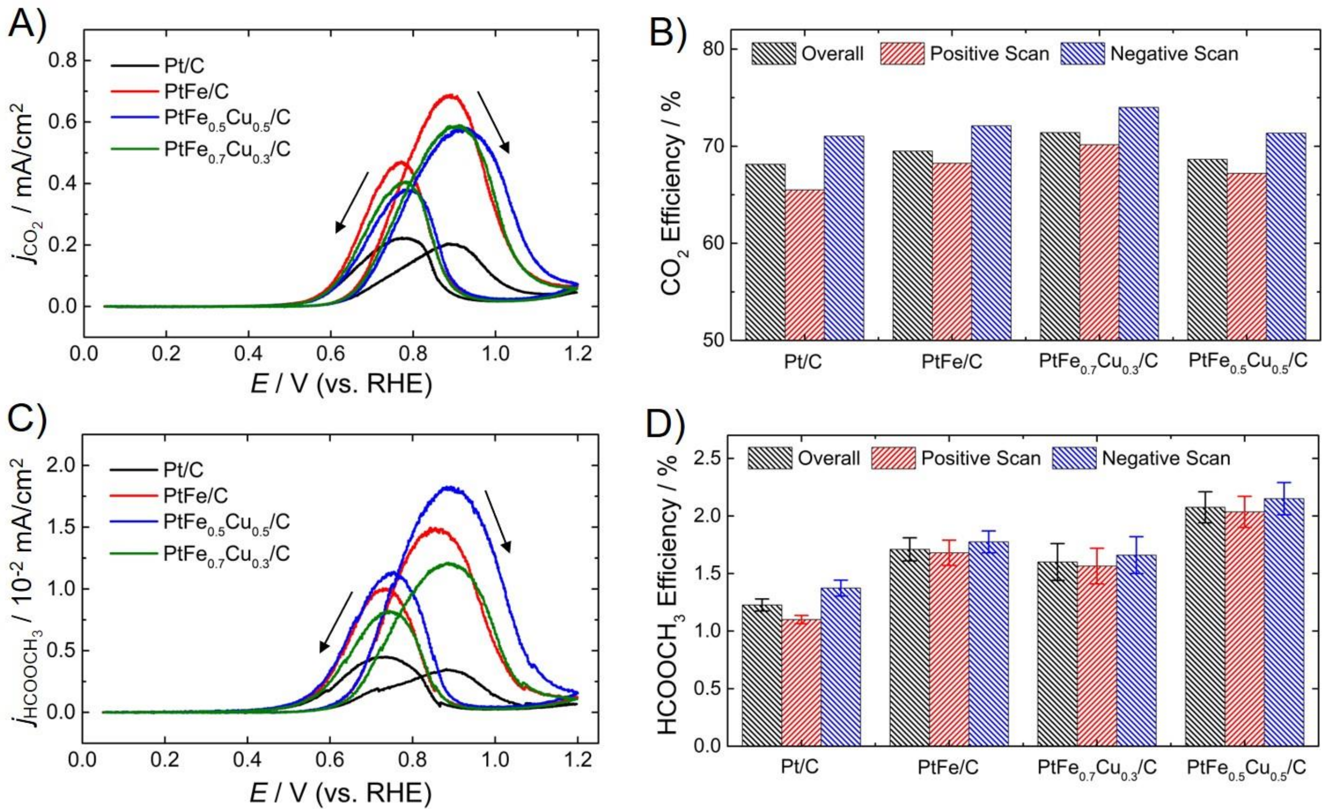

Figure 4. Cyclic voltammograms: (A) CO_2 partial current density. (B) Current efficiency of CO_2 in full, positive and negative cycles, respectively. (C) Methyl formate partial current density. (D) Current efficiency of methyl formate in full, positive and negative cycles, respectively. Scan rate: 10 mV/s, Flow rate: 10 μL/s. All the currents were normalized to the ECSA. The higher conversion efficiency in the negative direction may arise from effects of chemical reaction.

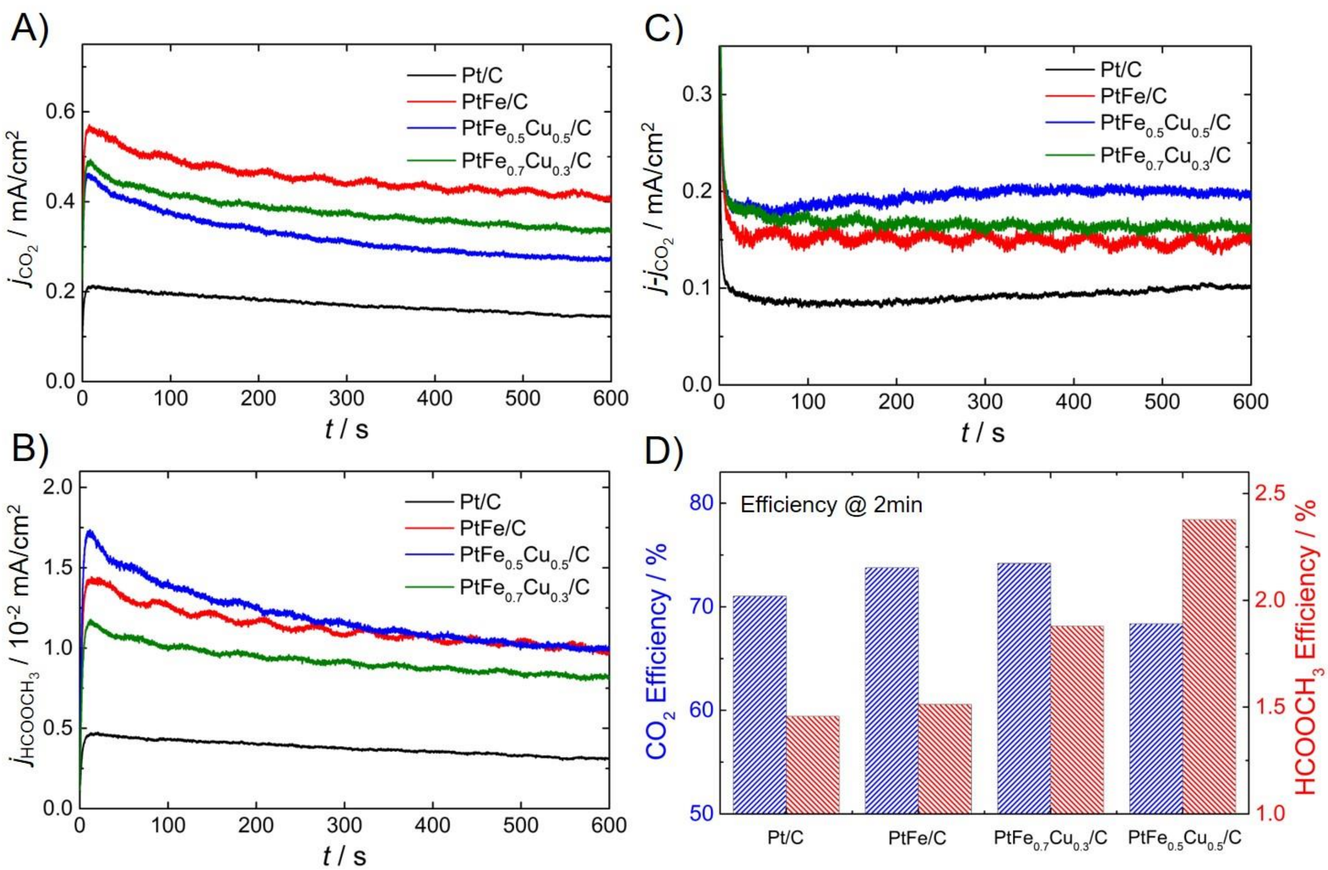

Figure 5. Chronoamperometry at 0.80 V vs. RHE**:** (A) CO_2 partial current density. (B) Methyl formate partial current density. (C) Overall current density excluding CO_2, representing the formation of formic acid and formaldehyde. (D) Current efficiency at 2 min during polarization. Flow rate: 10 μL/s. All the currents were normalized to the ECSA. The current efficiencies for CO_2 and methyl formate show a decay during testing.

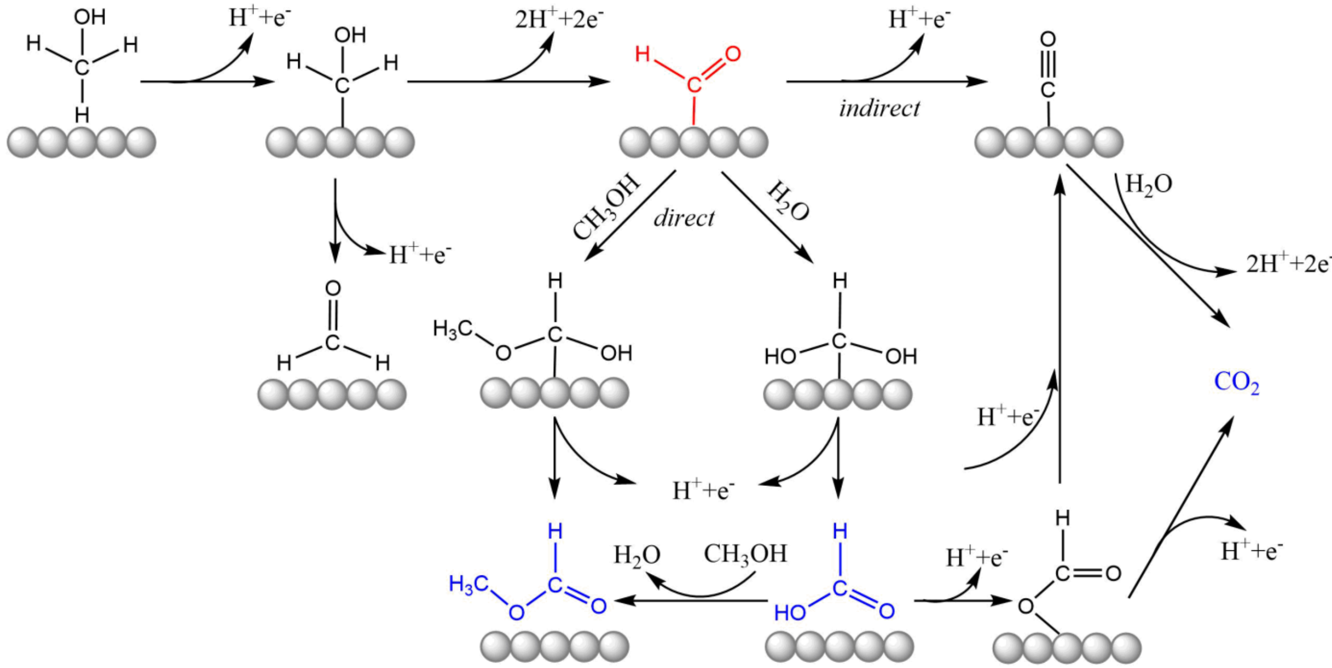

Scheme 1. Proposed reaction mechanism for methanol oxidation. The adsorbed HCO species determines whether the reaction proceeds via the indirect or direct pathway. An increase in the lattice compressive strain may lower the energy barriers for forming adsorbed $HCOHOCH_3$ or $HC(OH)_2$ while adsorbed CO is affected in a non-monotonic way.

REFERENCES

(1) Staffell, I.; Scamman, D.; Velazquez Abad, A.; Balcombe, P.; Dodds, P. E.; Ekins, P.; Shah, N.; Ward, K. R. The Role of Hydrogen and Fuel Cells in the Global Energy System. *Energy Environ. Sci.* **2019**, *12*, 463–491.

(2) Kakati, N.; Maiti, J.; Lee, S. H.; Jee, S. H.; Viswanathan, B.; Yoon, Y. S. Anode Catalysts for Direct Methanol Fuel Cells in Acidic Media: Do We Have Any Alternative for Pt or Pt-Ru? *Chem. Rev.* **2014**, *114*, 12397–12429.

(3) Watanabe, M.; Motoo, S. Electrocatalysis by Ad-Atoms: Part II. Enhancement of the Oxidation of Methanol on Platinum by Ruthenium Ad-Atoms. *J. Electroanal. Chem. Interfacial Electrochem.* **1975**, *60*, 267–273.

(4) Waszczuk, P.; Wieckowski, A.; Zelenay, P.; Gottesfeld, S.; Coutanceau, C.; Léger, J.-M.; Lamy, C. Adsorption of CO Poison on Fuel Cell Nanoparticle Electrodes from Methanol Solutions: A Radioactive Labeling Study. *J. Electroanal. Chem.* **2001**, *511*, 55–64.

(5) Wasmus, S.; Tryk, D. A.; Vielstich, W. Electrochemical Behavior of Nitromethane and Its Influence on the Electro-Oxidation of Formic Acid: An On-Line MS Study. *J. Electroanal. Chem.* **1994**, *377*, 205–214.

(6) Wang, H.; Alden, L.; DiSalvo, F. J.; Abruña, H. D. Electrocatalytic Mechanism and Kinetics of SOMs Oxidation on Ordered PtPb and PtBi Intermetallic Compounds: DEMS and FTIRS Study. *Phys. Chem. Chem. Phys.* **2008**, *10*, 3739–3751.

(7) Huang, L.; Zhang, X.; Wang, Q.; Han, Y.; Fang, Y.; Dong, S. Shape-Control of Pt–Ru Nanocrystals: Tuning Surface Structure for Enhanced Electrocatalytic Methanol Oxidation. *J. Am. Chem. Soc.* **2018**, *140*, 1142–1147.

(8) Marković, N. M.; Gasteiger, H. A.; Ross, P. N.; Jiang, X.; Villegas, I.; Weaver, M. J. Electro-Oxidation Mechanisms of Methanol and Formic Acid on Pt-Ru Alloy Surfaces. *Electrochim. Acta* **1995**, *40*, 91–98.

(9) Zhao, X.; Yin, M.; Ma, L.; Liang, L.; Liu, C.; Liao, J.; Lu, T.; Xing, W. Recent Advances in

Catalysts for Direct Methanol Fuel Cells. *Energy Environ. Sci.* **2011**, *4*, 2736–2753.

(10) Miura, A.; Wang, H.; Leonard, B. M.; Abruña, H. D.; DiSalvo, F. J. Synthesis of Intermetallic PtZn Nanoparticles by Reaction of Pt Nanoparticles with Zn Vapor and Their Application as Fuel Cell Catalysts. *Chem. Mater.* **2009**, *21*, 2661–2667.

(11) Wang, D.; Xin, H. L.; Hovden, R.; Wang, H.; Yu, Y.; Muller, D. A.; DiSalvo, F. J.; Abruña, H. D. Structurally Ordered Intermetallic Platinum–Cobalt Core–Shell Nanoparticles with Enhanced Activity and Stability as Oxygen Reduction Electrocatalysts. *Nat. Mater.* **2013**, *12*, 81–87.

(12) Maksimuk, S.; Yang, S.; Peng, Z.; Yang, H. Synthesis and Characterization of Ordered Intermetallic PtPb Nanorods. *J. Am. Chem. Soc.* **2007**, *129*, 8684–8685.

(13) Qi, Z.; Xiao, C.; Liu, C.; Goh, T. W.; Zhou, L.; Maligal-Ganesh, R.; Pei, Y.; Li, X.; Curtiss, L. A.; Huang, W. Sub-4 nm PtZn Intermetallic Nanoparticles for Enhanced Mass and Specific Activities in Catalytic Electrooxidation Reaction. *J. Am. Chem. Soc.* **2017**, *139*, 4762–4768.

(14) Cui, Z.; Chen, H.; Zhao, M.; Marshall, D.; Yu, Y.; Abruña, H.; Disalvo, F. J. Synthesis of Structurally Ordered Pt_3Ti and Pt_3V Nanoparticles as Methanol Oxidation Catalysts. *J. Am. Chem. Soc.* **2014**, *136*, 10206–10209.

(15) Zhu, J.; Yang, Y.; Chen, L.; Xiao, W.; Liu, H.; Abruña, H. D.; Wang, D. Copper-Induced Formation of Structurally Ordered Pt–Fe–Cu Ternary Intermetallic Electrocatalysts with Tunable Phase Structure and Improved Stability. *Chem. Mater.* **2018**, *30*, 5987–5995.

(16) Baltruschat, H. Differential Electrochemical Mass Spectrometry. *J. Am. Soc. Mass Spectrom.* **2004**, *15*, 1693–1706.

(17) Oberacher, H.; Pitterl, F.; Erb, R.; Plattner, S. Mass Spectrometric Methods for Monitoring Redox Processes in Electrochemical Cells. *Mass Spectrom. Rev.* **2015**, *34*, 64–92.

(18) Heinen, M.; Chen, Y. X.; Jusys, Z.; Behm, R. J. In Situ ATR-FTIRS Coupled with on-Line DEMS under Controlled Mass Transport Conditions—A Novel Tool for Electrocatalytic Reaction Studies. *Electrochim. Acta* **2007**, *52*, 5634–5643.

(19) Brimaud, S.; Jusys, Z.; Behm, R. J. Shape-Selected Nanocrystals for in situ Spectro-

Electrochemistry Studies on Structurally Well Defined Surfaces under Controlled Electrolyte Transport: A Combined in situ ATR-FTIR/Online DEMS Investigation of CO Electrooxidation on Pt. *Beilstein J. Nanotechnol.* **2014**, *5*, 735–746.

(20) Jusys, Z.; Massong, H.; Baltruschat, H. A New Approach for Simultaneous DEMS and EQCM: Electro-Oxidation of Adsorbed CO on Pt and Pt-Ru. *J. Electrochem. Soc.* **1999**, *146*, 1093–1098.

(21) Jusys, Z.; Kaiser, J.; Behm, R. J. Composition and Activity of High Surface Area PtRu Catalysts towards Adsorbed CO and Methanol Electrooxidation—A DEMS Study. *Electrochim. Acta* **2002**, *47*, 3693–3706.

(22) Jusys, Z.; Kaiser, J.; Behm, R. J. Methanol Electrooxidation over Pt/C Fuel Cell Catalysts: Dependence of Product Yields on Catalyst Loading. *Langmuir* **2003**, *19*, 6759–6769.

(23) Wang, H.; Wingender, C.; Baltruschat, H.; Lopez, M.; Reetz, M. T. Methanol Oxidation on Pt, PtRu, and Colloidal Pt Electrocatalysts: A DEMS Study of Product Formation. *J. Electroanal. Chem.* **2001**, *509*, 163–169.

(24) Celorrio, V.; Plana, D.; Flórez-Montaño, J.; Montes de Oca, M. G.; Moore, A.; Lázaro, M. J.; Pastor, E.; Fermín, D. J. Methanol Oxidation at Diamond-Supported Pt Nanoparticles: Effect of the Diamond Surface Termination. *J. Phys. Chem. C* **2013**, *117*, 21735–21742.

(25) Samjeské, G.; Wang, H.; Löffler, T.; Baltruschat, H. CO and Methanol Oxidation at Pt-Electrodes Modified by Mo. *Electrochim. Acta* **2002**, *47*, 3681–3692.

(26) Zhao, Y.; Li, X.; Schechter, J. M.; Yang, Y. Revisiting the Oxidation Peak in the Cathodic Scan of the Cyclic Voltammogram of Alcohol Oxidation on Noble Metal Electrodes. *RSC Adv.* **2016**, *6*, 5384–5390.

(27) Jambunathan, K.; Jayaraman, S.; Hillier, A. C. A Multielectrode Electrochemical and Scanning Differential Electrochemical Mass Spectrometry Study of Methanol Oxidation on Electrodeposited Pt_xRu_y. *Langmuir* **2004**, *20*, 1856–1863.

(28) Abd-El-Latif, A. A.; Baltruschat, H. Formation of Methylformate during Methanol Oxidation Revisited: The Mechanism. *J. Electroanal. Chem.* **2011**, *662*, 204–212.

(29) Mostafa, E.; Abd-El-Latif, A.-E.-A. A.; Baltruschat, H. Electrocatalytic Oxidation and Adsorption Rate of Methanol at Pt Stepped Single-Crystal Electrodes and Effect of Ru Step Decoration: A DEMS Study. *ChemPhysChem* **2014**, *15*, 2029–2043.

(30) Wang, H.; Baltruschat, H. DEMS Study on Methanol Oxidation at Poly- and Monocrystalline Platinum Electrodes: The Effect of Anion, Temperature, Surface Structure, Ru Adatom, and Potential. *J. Phys. Chem. C* **2007**, *111*, 7038–7048.

(31) Bergamaski, K.; Pinheiro, A. L. N.; Teixeira-Neto, E.; Nart, F. C. Nanoparticle Size Effects on Methanol Electrochemical Oxidation on Carbon Supported Platinum Catalysts. *J. Phys. Chem. B* **2006**, *110*, 19271–19279.

(32) Wang, H.; Alden, L. R.; DiSalvo, F. J.; Abruña, H. D. Methanol Electrooxidation on PtRu Bulk Alloys and Carbon-Supported PtRu Nanoparticle Catalysts: A Quantitative DEMS Study. *Langmuir* **2009**, *25*, 7725–7735.

(33) Nagao, R.; Cantane, D. A.; Lima, F. H. B.; Varela, H. The Dual Pathway in Action: Decoupling Parallel Routes for CO_2 Production during the Oscillatory Electro-Oxidation of Methanol. *Phys. Chem. Chem. Phys.* **2012**, *14*, 8294–8298.

(34) Schnur, S.; Groß, A. Strain and Coordination Effects in the Adsorption Properties of Early Transition Metals: A Density-Functional Theory Study. *Phys. Rev. B* **2010**, *81*, 033402–033402.

For Table of Contents Only